Study of a sol-gel precursor and its evolution towards ZnO

Alberto Gómez-Núñez[1], Concepción López[2], Santiago Alonso-Gil[3], Pere Roura[4], Anna Vilà[1]*

[1]University of Barcelona, Department of Electronics, Martí i Franquès 1, E08028-Barcelona, Spain.

[2]University of Barcelona, Department of Inorganic Chemistry, Martí i Franquès 1, E08028-Barcelona, Spain.

[3]University of Barcelona, Department of Organic Chemistry, Martí i Franquès 1, E08028-Barcelona, Spain.

[4]University of Girona, Department of Physics, Campus Montilivi, Edif. PII, E17071-Girona, Spain.

*Corresponding author: Phone: +34934039170, Fax: +34934021148, avila@el.ub.edu, anna.vila@ub.edu

Keywords: oxides; heat treatment; infrared spectroscopy (IR); X-ray diffraction; thermogravimetric analysis (TGA); ab initio calculations.

Abstract: The processes involved in the assembly of zinc acetate dihydrate {$Zn(CH_3COO)_2 \cdot 2H_2O$} and ethanolamine ($H_2NCH_2CH_2OH$), with or without 2-methoxyethanol as solvent, have been analysed by infrared spectra, mass spectrometry, nuclear magnetic resonance, powder X-ray diffraction and computational studies. Thermal evolution of the mixtures was characterized by thermoanalytical and structural techniques (thermogravimetry, differential thermal analysis, differential scanning calorimetry, X-ray diffraction and X-Ray photoelectron spectroscopy). Computational studies together with experiments served to thoroughly describe the precursor and its decomposition. The thermal decomposition of the mixture and its transformation into crystalline ZnO take place in a temperature range between 50 and 450 °C through different processes. With solvent, the processes need temperatures 90 ^{o}C higher with respect to the mixture without solvent, and ZnO arises at 250 ^{o}C.

INTRODUCTION

ZnO has tremendous interest because of its applications in a variety of fields such as surface acoustic-wave devices, photonic crystals, photodetectors, photodiodes, varistors, transparent electronics, chemical sensors or solar cells. It has a direct energy band gap of 3.37 eV and it is a promising material for light emiting devices in many spectral regions. ZnO properties are well studied[1-5]. The sol–gel deposition

method[6] is routinely used, but the details of the process are still controversial. Some works demonstrate the huge influence that ambient humidity[7], precursor[8] or solvent[9] have on the pyrolysis of zinc acetate dihydrate (ZAD) and the subsequent formation of ZnO[10,11,12]. Other reports highlight the appearance of different intermediate compounds, such as hydroxyl- or anhydrous acetates[13], oxo-acetates[14] or hydrated hydroxyl-acetates[15] when similar ZAD species degrade, giving rise to nanowires[16], nanobelts[17] or other nanostructures[18,19,20].

The synthesis and thermal treatment of precursors to obtain a very well crystalline ZnO film as seeding layer for the further growth of vertically oriented ZnO nanowires is crucial. Deep studies of the synthesis conditions (crystallization temperature, deposition method, concentration …) of zinc acetate is responsible of a well crystalline film and then of nice ZnO nanowires[21, 22].

Search for the sol-gel precursor to minimize problems related with solubility or high temperature decomposition is a key point for this evolving technology. Various precursors involving ZAD mixed with nitrogen-based organic compounds have been studied[23,24], demonstrating that these mixtures evolve towards periodic oligomer molecules. In these cases, aminoalcohols are expected to bridge zinc-acetate units in a single molecule, thus covering the metal-oxygen core with an organic shell and making it more soluble in non-polar solvents. Other works add a stabilizer to the precursor[25-28]. Nevertheless, the detailed progress from solution towards crystalline ZnO is still ambiguous.

In this work we focus on the evolution from the usual initial solution (ZAD plus stabilizer) to the final structure of the ZnO obtained after thermal treatment. We pay attention to the processes involved in the assembly of the precursor, its crystal structure and thermal decomposition, thoroughly controlling the ZnO formation. The influence of the solvent will be also analyzed.

EXPERIMENTAL PROCEDURE

Samples preparation

Zinc acetate dihydrate [$Zn(CH_3COO)_2 \cdot 2H_2O$, ZAD], ethanolamine ($H_2NCH_2CH_2OH$, EA) and 2-methoxyethanol [$CH_3O(CH_2)_2OH$, ME] were purchased from Panreac, Acrös Organics and Aldrich, respectively, and used as received.

The two samples used in this study (hereinafter referred to as “Precursor” and “Ink”) were prepared as follows:

- **Synthesis of the Precursor**: ZAD (1.8 g, 7.7×10^{-3} mol) was treated with an equimolar[29,30] amount of EA (0.47 mL)**.** The mixture was kept at 60 °C under continuous stirring for 24 h. After this period the flask containing the homogeneous gel was stored in a silica gel desiccator for several days until a powder was formed.
- **Preparation of the Ink**: This sample, suitable for printed electronics, was prepared as described for the Precursor but adding ME (7 mL) as solvent.

Ink thin films were prepared by the drop coating method on a glass substrate.

Characterization, Structural, Thermal and Computational details

The as-obtained Precursor was characterized by Infrared (IR) spectroscopy, ^{1}H and $^{13}C\{^{1}H\}$ Nuclear Magnetic Resonance (NMR) and Mass Spectrometry (MS). IR spectra were registered with a Nicolet 400FTIR instrument using KBr pellets. ^{1}H and $^{13}C\{^{1}H\}$ NMR studies were carried out at 25 °C by a Mercury-400 MHz instrument using $CDCl_3$ (99.9 %) as solvent and $SiMe_4$ as reference. ESI^{+}-MS was performed with a LC/MSD-TOF (Agilent Technologies) mass spectrometer. The dried Precursor powder was characterized by X-ray diffraction (XRD) in a PANalytical X'Pert PRO MPD θ/θ powder diffractometer, with Cu $K\alpha_1$ radiation (λ = 1.5406 Å) in a convergent-beam configuration with a transmission geometry.

To study the thermal evolution of both Precursor and Ink, Thermogravimetric Analyses (TGA), Differential Scanning Calorimetry (DSC) and Differential Thermal Analyses (DTA) were carried out in an atmosphere of dry air with 50 mL/min flow rate and heating rate of 10 °C/min up to 600 °C. DSC was performed by a Mettler-Toledo DSC-822e calorimeter, with uncovered aluminium crucibles (of 40 µL volume). TGA experiments were performed on a Mettler-Toledo TGA-851e thermobalance, also with uncovered aluminium crucibles (of 70 µL volume). Complementary Evolved Gas Analysis (EGA) of the evolved species (up to *m/z* = 70) was done by coupling a mass spectrometer at the exit of the TGA apparatus. A MKS quadrupole mass spectrometer (Microvision Plus) was used.

The evolution of the crystalline structure with temperature was analysed by *in-situ* and *ex-situ* (for Precursor and Ink, respectively) XRD experiments. In *ex-situ* measurements, the desiccated powders were heated inside the TG furnace at 10 °C/min up to the desired temperature and then cooled down without any delay. A new sample was used for each temperature. In contrast, *in-situ* experiments were carried out on one single Ink sample that was held during 8 min. at isothermal conditions (to allow for an XRD

measurement) every 10 ^{o}C, with a high-temperature camera (HTK – 1200N, Antoon Paar). The heating rate between isotherms was 10 ^{o}C/min from room temperature to 600 ^{o}C, what resulted in an average heating rate of 1.1 ^{o}C/min, i.e. much slower than for *ex-situ* experiments.

The deposited Ink was analyzed by X-Ray photoelectron spectroscopy (XPS) in a ultra-high vacuum (UHV) chamber using a PHI 5500 Multitechnique System (from Physical Electronics) with a monochromatic X-ray source (Al Kα line of 1486.6 eV energy and 350 W), placed perpendicular to the analyser axis and calibrated using the 3d5/2 line of Ag with a full width at half maximum (FWHM) of 0.8 eV. The selected resolution for the spectra was 187.85eV of Pass Energy and 0.8 eV/step for the general spectra and 23.5 eV of Pass Energy and 0.1 eV/step for the spectra of the different elements in the depth profile spectra. A low energy electron gun (less than 10 eV) was used in order to discharge the surface when necessary. The Ink films were heated at a constant rate of 10 ^{o}C/min up to several maximum temperatures and cooled down without any delay before the XPS measurements.

Computational studies (optimization of the geometries, calculation of total and free energies and frequencies) were performed with UB3LYP method implemented in the Gaussian 03[31] software, using the LANLD2Z basis set.

RESULTS AND DISCUSSION

Characterization of the Precursor

As stated above, the Precursor was characterized by IR, ^{1}H and ^{13}C{^{1}H}-NMR and mass spectrometry. Figure 1 shows the IR spectra obtained for the Precursor and ZAD. A larger separation between asymmetric and symmetric stretching bands of the carboxylate unit (ν_{as} and ν_{s}, respectively) is detected for the Precursor than for ZAD. According to the bibliography[32], this indicates the existence of bridging acetate ligands in the Precursor.

In the ^{1}H NMR spectrum of the Precursor (Figure 2), the signal due to the –NH_2 protons (around 3.6 ppm) is broad and shifted in relation to EA. Moreover, some changes are detected in chemical shifts and multiplicities of the resonances of the -$(CH_2)_2$- protons (around 2.85 ppm), when compared with those of the free ligand. These differences suggest, according to the literature[33,34], the presence of "[Zn{κ^2-*N,O*-(H_2N-$(CH_2)_2$O)}]" cores that arise from the binding of the amine nitrogen and the deprotonated oxygen to the Zn(II) cation. In addition, the singlet at $\delta \approx 2.1$ ppm is attributed to the acetato- ligand.

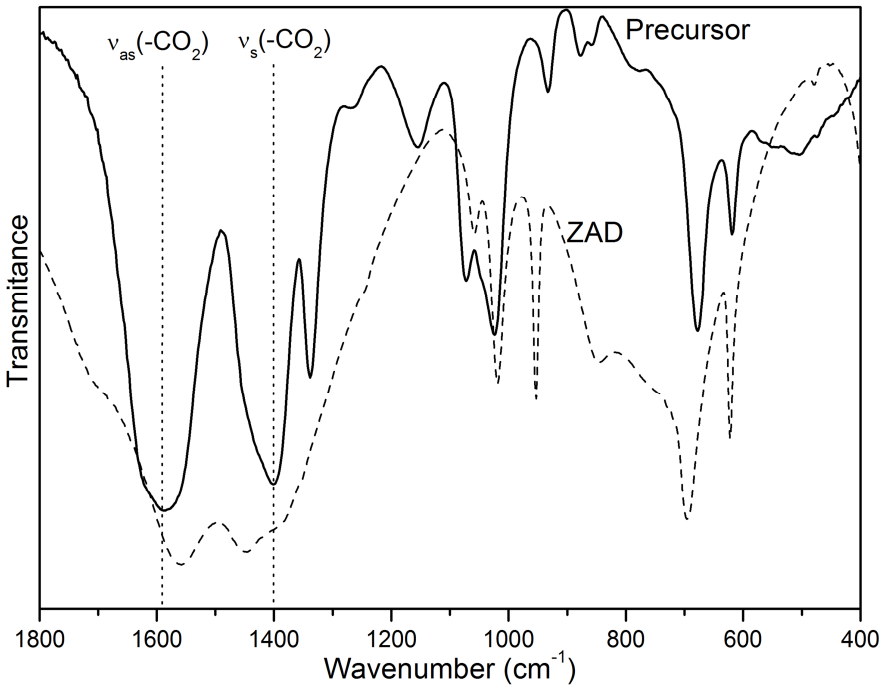

Figure 1. Infrared spectra (in the range 1800-400 cm^{-1}) of ZAD (dashed line) and the Precursor (solid line). The bands due to asymmetric (ν_{as}) and symmetric (ν_s) stretching modes of the carboxylate unit in the Precursor are marked.

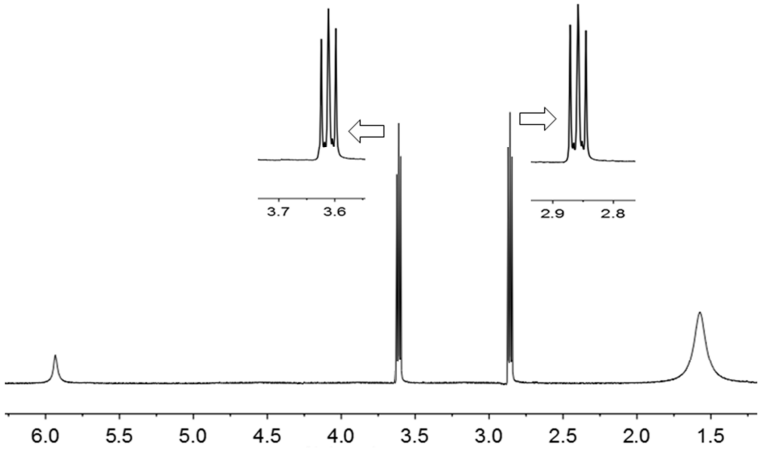

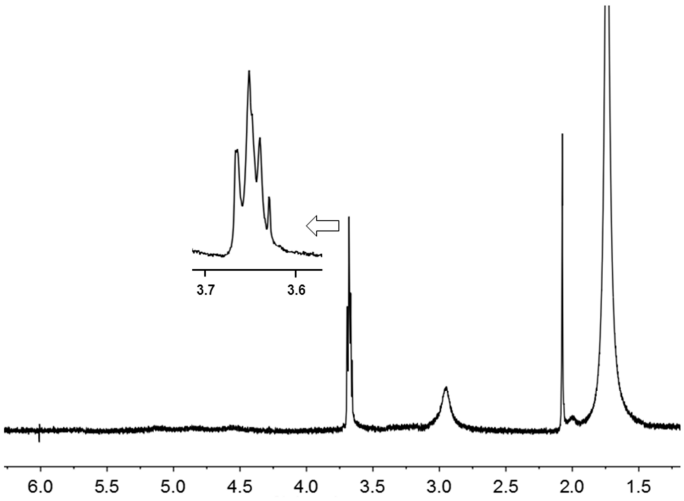

Figure 2. ^{1}H-NMR spectra (400 MHz) of ethanolamine (EA) (top) and the Precursor (bottom). The intense signal that appears in the spectrum of the Precursor in the range 1.5 ppm ≤ δ ≤ 1.8 ppm is due to the residual water of the solvent.

The $^{13}C\{^{1}H\}$ NMR spectrum of Precursor (Figure 3) shows four singlets, of which those at lower and higher fields are due to the acetate ligand; while the remaining two correspond to the -CH_2- carbons of the coordinated EA. It should be noted that the chemical shifts of these resonances were not coincident with those of the free ZAD or EA.

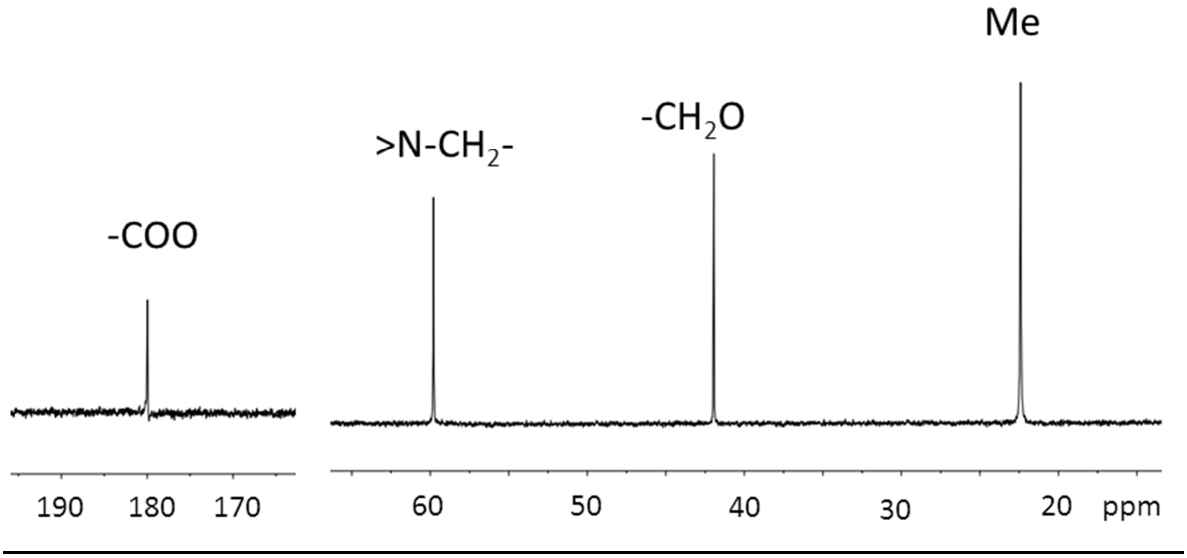

Figure 3. Partial views of the $^{13}C\{^{1}H\}$-NMR spectrum of the Precursor in $CDCl_3$ at 25 ^{o}C.

All these findings suggest that ZAD interacts with EA, giving rise to new species in which the environment of the metal centre is "$Zn(H_2NCH_2CH_2O)(\mu\text{-}OAc)$". It is well-known that these monomeric arrays may assemble giving polymetallic complexes of higher nuclearity. Some authors have postulated the formation of tetranuclear and hexanuclear Zn(II) complexes containing simultaneously carboxylate and aminoalcoholate ligands. Only a few among these crystal structures have been determined by X-ray diffraction[23, 24, 35-37], and in most of them there is one H_2O molecule "trapped" in tetrametallic units.

Complementarily, the ESI^+-MS spectrum of the Precursor (Figure S1 in Supporting Information) shows peaks with the isotopic pattern expected for cations with different nuclearities: $[Zn]_x$ (with x = 2, 4 or 6) and $\{[Zn]_x + H_2O\}$. Unfortunately, data available do not allow stablishing whether these species arise by fragmentation of cations with higher nuclearity or by assembly of smaller units (i.e. monomers or dimers). However, it is clear that only Zn dimers, tetramers and hexamers are compatible with our results, and XRD could help describing the exact composition resulting from the interaction between ZAD and EA.

Since attempts to obtain single crystals suitable for X-ray diffraction failed, powder XRD studies of the dried precursor were performed (Exp. day 1 in Figure 4). Indexation of the peaks observed in the spectrum is consistent with a monoclinic system and Z = 16. The lack of (0 k 0) reflexions with k = odd values indicates that the space group is $P2_1$. As shown in Fig. 4, the experimental XRD spectrum of freshly-prepared dried Precursor matches with the calculated one for the Monoclinic $P2_1/m$ system, although after a few days at room conditions of temperature and humidity, the Precursor becomes amorphous (Exp. day 5 in Fig. 4). However, the $P2_1/m$ system is centrosymmetric and implies 4 asymmetric units, what, since Z = 16, indicates that only $[Zn]_x$ with x = 4 is possible in fresh Precursor. As a conclusion, the present structure must be made from four tetramers ($4[Zn]_4$), in good agreement with the literature[37].

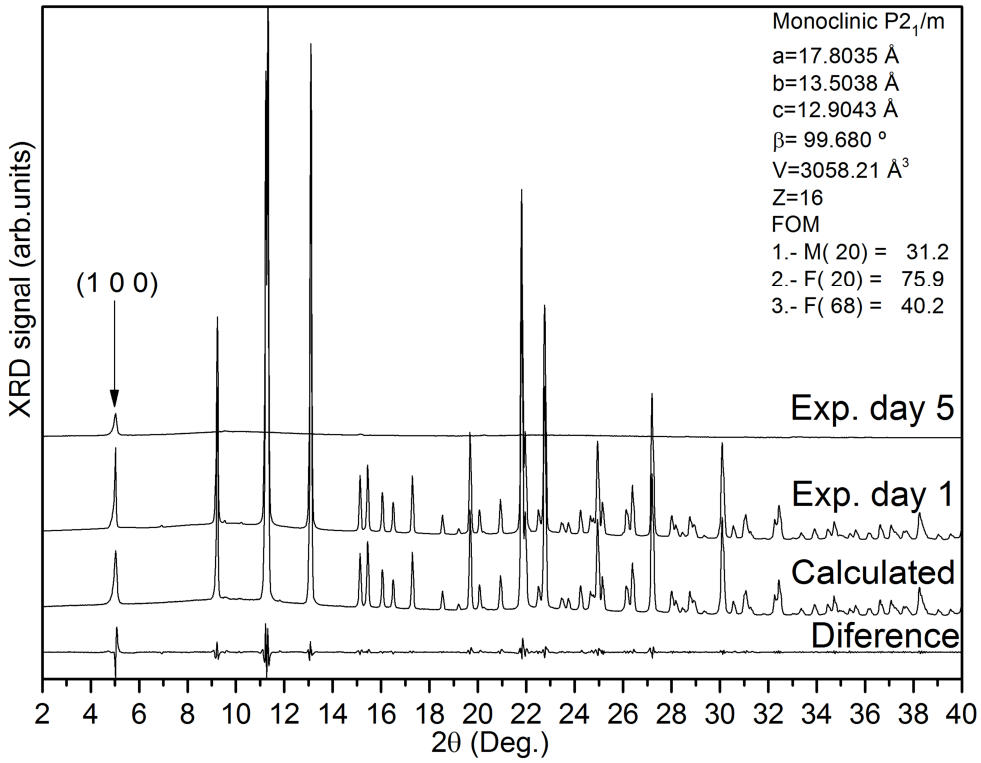

Figure 4. Experimental XRD spectrum of freshly-obtained Precursor (Exp. day 1), calculated diffractogram for a monoclinic $P2_1/m$ system with the parameters shown at the upper-right corner, and the difference between both. After five days of storage at room conditions (Exp. day 5) only the (100) reflection remains.

Computational study of the Precursor

In order to understand why small mononuclear ($[Zn]_1$) or dinuclear ($[Zn]_2$) blocks assemble to form $[Zn]_4$ oligomers compatible with XRD results, computational studies were undertaken. In a first stage, the geometries of the $[Zn]_x$ entities (x = 1, 2 or 4) were optimized (Fig. 5) by means of Gaussian 03 software. In the three cases bond lengths and angles of the optimized geometries were consistent with those reported for other Zn(II) complexes with identical sets of donor atoms[37]. Vibrational calculations were also carried out, and no peaks at negative frequencies appeared, indicating that these systems remained at the minimum state of the Potential Energy Surface.

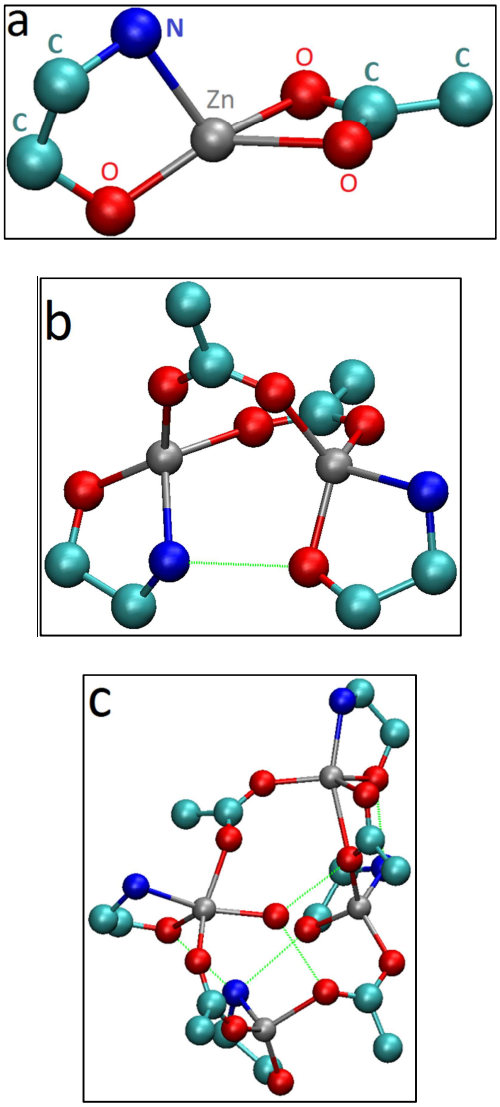

Figure 5. Optimized geometries of the monomer ($[Zn]_1$, a), dimer ($[Zn]_2$, b) and tetramer ($[Zn]_4$, c) using UB3LYP method and LANLD2DZ base. Hydrogen atoms have been omitted for clarity.

On the other hand, calculations of free energy (ΔG) suggest that each individual tetramer is much more stable than two isolated dimers or four monomers, indicating that tetramers are the stable form for this type of system. Referring to their formation, binary collision (two monomers into a dimer or two dimers into a tetramer) is kinetically more probable than quaternary collision (four monomers into a tetramer). Furthermore, calculated free energies at 300 K were used to estimate the ΔG for the assembly of: a) 2

dimers or b) 4 monomers to give the tetramer. The results showed that ΔG of process a) is (ca. 33 Kcal / mol) smaller than that of b), thus indicating that tetramers coming from the union of two dimers with a water molecule are the stable form for this type of system, in good agreement with our experimental results and with crystal structures of similar Zn-carboxilate aminoalcohol compounds.

Comparative studies of the thermal evolution of the Precursor and the Ink

Once the Precursor has been fully characterized, research has been focused on its thermal behavior and the influence of the solvent (ME) on it. To this aim, TGA analyses were performed for both the Ink and the Precursor.

As depicted in Figure 6, the Ink undergoes a very pronounced mass-loss process (step A), that is not observed for the Precursor, near the boiling point of ME (120 ^{o}C) that is attributed to solvent evaporation. At higher temperatures, TGA curves of both Ink and Precursor also show two additional mass-loss steps (B and C) at around 170 and 230 ^{o}C respectively, but with different relative heights. This feature deformations, together with the clear shape difference of the additional higher-temperature step D (290 ^{o}C) in the Ink curve (see the Inset of Fig. 6), makes evident that the residual ME solvent has an effect on the oligomers decomposition.

The final mass measured after the Precursor decomposition (m_f = 0.31 m_i) is very close to the one expected for the transformation of an equimolar mixture of ZAD and EA into ZnO (m_F = 0.29m_i). It can be concluded that, in contrast with studies carried out on pure ZAD[7], no Zn loss occurred during decomposition, as if interaction with EA prevented it.

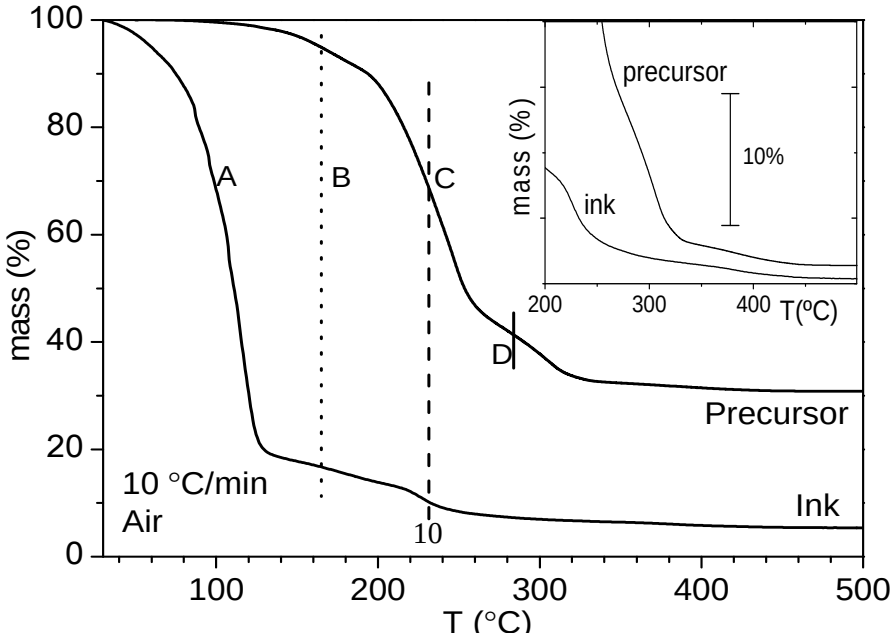

Figure 6. TGA curves of Ink and Precursor. Step A is due to ME evaporation whereas steps B, C and D correspond to decomposition. An expansion of the plot in the range 200-500 °C is shown as an inset.

Simultaneous DTA and EGA signals recorded during the TG experiment[38-41] on the Precursor have been used to deduce some general characteristics of the oligomers decomposition process (steps B, C and D). First of all, since DTA signal (not shown) is always endothermic, it is sure that decomposition proceeds without substantial oxidation of the organic ligands. This conclusion is reinforced by the fact that CO_2 (*m/z* = 44) begins to evolve after the two main decomposition steps (Figure 7). In fact, steps B and C do no correlate with any EGA peak despite that most of the mass is lost during step C. It can be concluded that these steps involve evolution of large fragments that cannot be detected with the present experimental setup (having *m/z* > 70). Finally, the last step D correlates with peaks of *m/z* = 44 and *m/z* = 43, that correspond to CO_2 and to the superposition of acetone and other volatile signatures. Most of these volatiles have been also detected in previous studies on the thermal stability of Zn(II) complexes and have been ascribed to the formation of cyclic nitrogen-species[42].

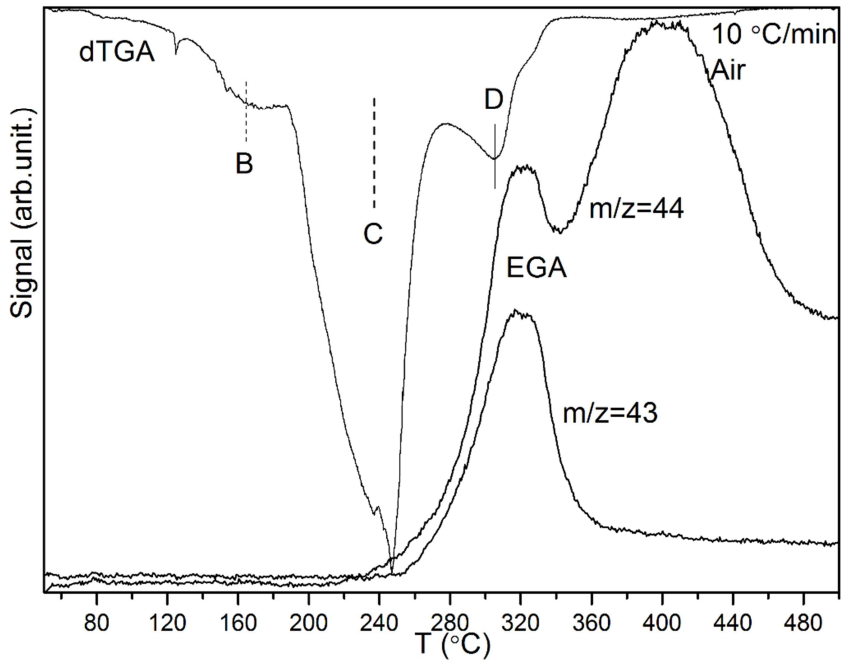

Figure 7. Derivative of the TGA (dTGA, thin line) curve and coupled MS signals (EGA, thick lines) for *m/z* = 43 and *m/z* = 44 of the Precursor.

Evolution of the crystalline structure with the temperature

To study the evolution of the crystalline structure, we performed additional *in-situ* and *ex-situ* XRD experiments on the dried Precursor and Ink, respectively, at temperatures up to 600 ^{o}C (Figure 8). As shown in Fig. 8a, the dried Precursor is highly crystalline at room temperature, it becomes amorphous for temperatures higher than 80 ^{o}C and transforms into crystalline ZnO above 160 ^{o}C. This early formation of ZnO during the *in-situ* XRD experiments seems contradictory with the TGA measurements, where the Precursor decomposition process occurs in the 190-260 ^{o}C range. This different behaviour is probably due to: a) the more difficult gas exchange, and consequently slower decomposition rate[43], in a bulky sample (necessary for TG experiments) than for the layer needed for powder XRD; and b) the long stabilization time required for each *in-situ* XRD measurement, so the time in each temperature has an important role.

In contrast, the *ex-situ* XRD spectra obtained for the Ink (Fig. 8b) show that crystallinity of the initial phase steadily increases up to 210 ^{o}C, while in the range 210 - 270 ^{o}C it coexists with crystalline ZnO, that becomes the only phase above 270 ^{o}C, that is ca. 90 ^{o}C higher than the temperature required for the Precursor.

In situ

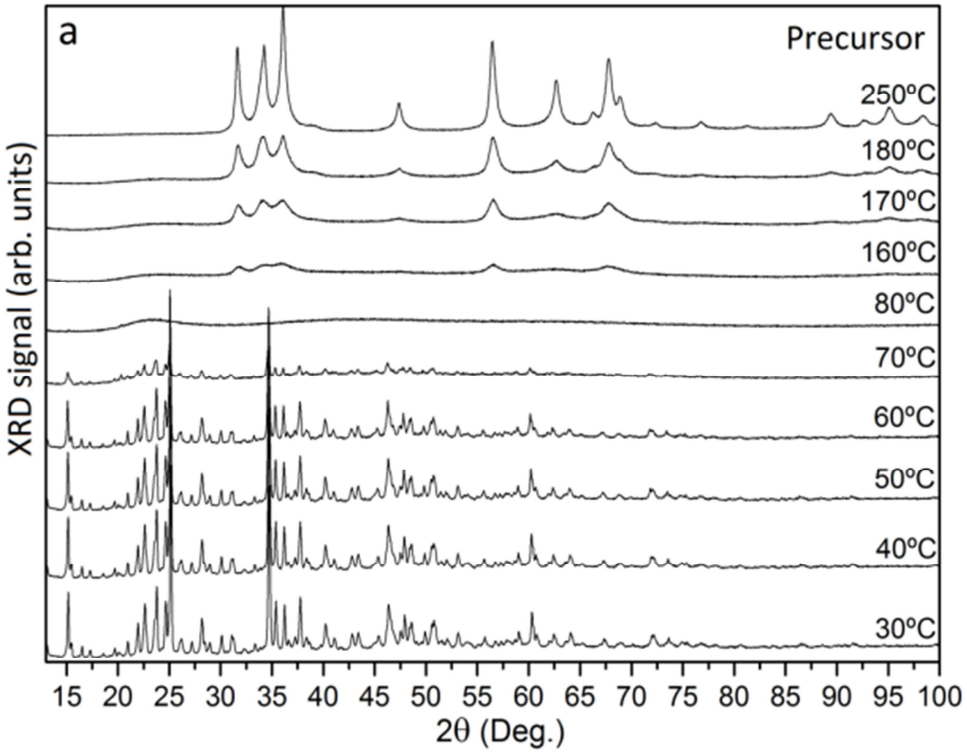

Ex situ

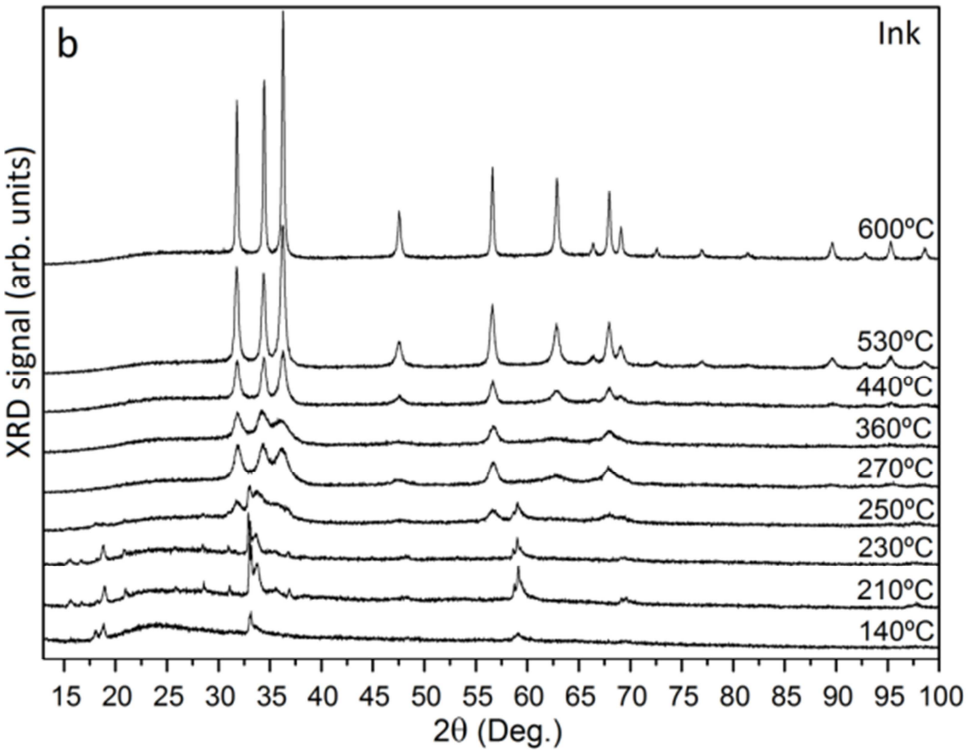

Figure 8. XRD spectra measured at various temperatures of: a) *in-situ* dried Precursor and b) *ex-situ* Ink.

Atomic environment

The structural evolution of the Ink has been further analyzed by looking at the atomic environment of the Zn, C, O and N atoms by XPS analyses of the Zn 2p, Zn LMM and O1s Auger lines at different temperatures (up to 600 °C). Modified Auger parameter, calculated from the binding energy of Zn $2p_{3/2}$ photoelectron peak and the kinetic energy of Zn $LM_{45}M_{45}$ Auger peak is similar to the one (2010 eV) reported in the NIST database for ZnO[44], above 250 ^{o}C. In addition, the atomic ratio between Zn and N varies from 1 to 5, from room temperature to 180 ºC (after steps A and B in TGA curves), respectively. From 180 ºC to 250 ºC, the Zn/N ratio increases above 20 (step C in TGA curves) and some few N remains at the Ink at T > 250 ^{o}C. Indeed, a weak N_{1s} signal still remains up to 600 ^{o}C, it is concluded that some N atoms remain after decomposition even at so high temperatures.

Table 1. Evolution of the area percentage for the deconvoluted O_{1s} lines at 530.0 eV (corresponding to Zn-O-Zn bonds) and 531.6 eV (O-H and O-C-O bonds) and Zn/N atomic ratio calculated after XPS measurements on the Ink at different temperatures.

Bonds	**BE O_{1s}(eV)**	**180 °C**	**210 °C**	**230 °C**	**250 °C**
Zn-O-Zn	530.0	19	21	24	39
O-H **O-C-O**	531.6	81	79	76	61

The evolution of the area percentage for the deconvoluted O_{1s} lines is summarized in Table 1. This deconvolution shows the presence of two different O_{1s} peaks. For ZnO, the 530 eV peak corresponds to O^{2-} ions surrounded by Zn atoms[45], and 531.6 eV to O^{2-} ions in the oxygen deficient regions and to OH bonds[46]. From 180 °C to 250 °C, when the ZnO just starts to crystallize according to XRD experiments, the main peak is that of organic-surrounded O^{2-} ions, whereas from 270 to 600 °C many organic species have evaporated and the main peak is associated to O^{2-} surrounded by Zn. Moreover, the thermal evolution of atomic concentration ratio between Zn and O reveals that, above 250 °C, ZnO becomes more stoichiometric: Zn/O varies from 0.6 to 0.9 up to 600 °C. These results are in good agreement with the fact that starting from 250 °C, crystal reconfiguration and last organic compound evaporations befall.

CONCLUSIONS

The detailed study of the system ZAD, EA as precursor, in the presence of ME as solvent, summarized in this work provides conclusive evidences for the roles of the stabilizer (EA) and the solvent (ME) in the formation of ZnO from ZAD. First, it has been proved that EA reacts with ZAD giving tetramers with "$Zn(H_2NCH_2CH_2O)(\mu\text{-}OAc)$" cores. Second, with ME an intermediate crystalline phase, not detected for the precursor (solvent-free system), appears below 270 °C and ZnO is formed at higher temperatures.

These studies constitute the first step for further work mainly centred on the investigation of the effects produced by other aminoalcohols and other solvents, which may be important to reduce the temperatures

required to achieve ZnO or to minimize solubility problems. These two aspects are relevant in view of the design of new procedures to achieve materials for technological applications such as printed electronics.

ASSOCIATED CONTENT

Supporting Information Available (PDF): Mass spectrum of the precursor (Figure S1) and Tables (S1–S4) containing a final atomic coordinates (*x*,*y*,*z*), ground-state and frequency data for the optimized geometries of the monomer, dimer and tetramer.

AUTHOR INFORMATION

Corresponding Author

* avila@el.ub.edu

Department of Electronics (UB), Martí i Franquès 1, E08028-Barcelona, Spain.

Telf. (+34) 93 403 91 70

Fax. (+34) 93 402 11 48

Author contributions

The manuscript was written through contributions of all authors. All authors have given approval to the final version of the manuscript.

AKNOWLEDGEMENTS

Angel Diéguez, Jordi Farjas, Paolo Pellegrino, Xavier Alcobé, Maria Barba, Paola Torche, Lorenzo Calvo, Laura Ortiz, Francisco Cárdenas, Cristina Puigjaner and the computer services of the Institute of Theoretical and Computational Chemistry of the University of Barcelona are acknowledged for their technical support and fruitful discussions.

REFERENCES

(1) Morkoç, H.; Özgür, Ü.; *Zinc oxide: Fundamentals, Materials and Device Technology*, Wiley-VCH, Weinheim, Germany, **2009**.

(2) Klingshirn, C.; *Phys. Stat. Sol. (b)*, **2007**, 244(9), 3027–3073.

(3) Klingshirn, C.; *ChemPhysChem*, **2007**, 8(6) 782–803.

(4) Janotti, A.; Van de Walle, C.G.; *Rep. Prog. Phys.*, **2009**, 72(12), 126501.

(5) Vaseem, M.; Umar, A.; Hahn, Y.-B.; *Metal Oxide Nanostructures and Their Applications*, **2009**, 4.

(6) Znaidi, L.; *Mat. Sci. Eng. B*, **2010**, 174, 18–30.

(7) Arii, T.; Kishi, A.; *Thermochim. Acta*, **2003**, 400(1–2), 175–185.

(8) Kumar, U.; Thomas, J.; Nagarajan, R.; Thirupathi, N.; *Inorg. Chim. Acta*, **2011**, 372(1), 191–199.

(9) Kanade, K.G.; Kale, B.B.; Aiyer, R.C.; Das, B.K.; *Mat. Res. Bull.*, **2006**, 41(3), 590–600.

(10) Kozawa, T.; Onda, A.; Yanagisawa, K.; Kishi, A.; Masuda, Y.; *Solid State Chem.*, **2011**, 184(3), 589–596.

(11) Ghule, A.V.; Ghule, K.; Chen, C.-Y.; Chen, W.-Y.; Tzing, S.-H.; Chang, H.; Lieng, Y.-C.; *J. Mass Spectrom.*, **2004**, 39(10), 1202–1208.

(12) Ghule, A.V.; Lo, B.; Tzing, S.-H.; Ghule, K.; Chang, H.; Ling, Y.C.; *Chem. Phys. Lett.*, **2003**, 381(3–4), 262–270.

(13) Biswick, T.; Jones, W.; Pacuła, A.; Serwicka, E.; Podobinski, J.; *Solid State Sci.*, **2009**, 11(2), 330–335.

(14) Labuayai, S.; Promarak, V.; Maensiri, S.; *Appl. Phys. A*, **2009**, 94(4), 755–761.

(15) Moezzi, A.; McDonagh, A.; Dowd, A.; Cortie, M.; *Inorg. Chem.*, **2013**, 52(1), 95–102.

(16) Lin, C-C.; Li, Y-Y.; *Mat. Chem. Phys.*, **2009**, 113(1), 334–337.

(17) Tarat, A.; Majithia, R.; Brown, R.A.; Penny, M.W.; Meissner, K.E.; Maffeis, T.G.G.; *Surf. Sci.*, **2012**, 606(7), 715–721.

(18) Wang, Y.; Li, Y.; Zhou, Z.; Zu, X.; Deng, Y.; *J. Nanopart. Res.*, **2011**, 13(10), 5193–5202.

(19) Yang, Y.; Chen, H.; Zhao, B.; Bao, X.; *J. Crystal Growth*, **2004**, 263(1), 447–453.

(20) Su, X.; Zhang, Z.; Wang, Y.; Zhu, M.; *J. Phys. D: Appl. Phys.*, **2005**, 38(21), 3934–3937.

(21) Farías Rivera, V.; Auras, F.; Motto, P.; Stassi, S.; Canavese, G.; Celasco, E.; Bein, T.; Onida, B.; Cauda, V.; *Chem. Eur. J.*, **2013**, 19(43), 14665–14674.

(22) Laurenti, M.; Cauda, V.; Gazia, R.; Fontana, M.; Farías Rivera, V.; Bianco, S.; Canavese, G.; *Eur. J. Inorg. Chem.*, **2013**, 2013(14), 2520–2527.

(23) Lalioti, N.; Raptopoulou, C.P.; Terzis, A.; Aliev, A.E.; Gerothanassis, I.P.;Manessi-Zoupa, E.; Perlepes, S.P.; *Angew. Chem. Int. Ed.*, **2001**, 40 (17), 3211–3214.

(24) Hamid, M.; Tahir, A.A.; Mazhar, M.; Ahmad, F.; Molloy, K.C.; Kociok-Kohn, G.; *Inorg. Chim. Acta*, **2008**, 361(1), 188–194.

(25) Schneider, J.J.; Hoffmann, R.C.; Engstler, J.; Soffke, O.; Jaegermann, W.; Issanin, A.; Klyszcz, A.; *Adv. Mater.*, **2008**, 20(18),3383–3387.

(26) Schneider, J.J.; Hoffmann, R.C.; Engstler, J.; Dilfer, S.; Klyszcz, A.; Erdem, E.; Jakes, P.; Eichel, R.A.; *J. Mater. Chem.*, **2009**, 19, 1449–1457.

(27) Wang, Y.S.; Thomas, P.J; O'Brien, P.; *J. Phys. Chem. B*, **2006**, 110(9), 4099–4104.

(28) Hoffmann, R.; Dilfer, S.; Issanin, A.; Schneider, J.J.; *Phys. Stat. Sol. (a)*, **2010**, 207(7), 1590–1595.

(29) Kim, K.; Kim, S.; Lee, S.Y.; *Curr. Appl. Phys.*, **2012**, 12 (2), 585–588.

(30) Znaidi, L.; Soler Illia, G.J.A.A.; Le Guennic, R.; Sánchez, C.; Kanaev, A.; *J. Sol-Gel Sci. Technol.*, **2003**, 26(1–3) 817–821.

(30) Ohyama, M.; Kozuka, H.; Yoko, T.; *Thin Solid Films*, **1997**, 306 (1–2), 78–85.

(31) Frisch, M.J.; Trucks, G.W.; Schlegel, H.B; Scuseria, G.E.; Robb, M.A.; Cheeseman, J.R.; Montgomery, J.A.; Vreven, Jr.T.; Kudin, K.N.; Burant, J.C.; Millam, J.M.; Iyengar, S.S.; Tomasi, J.; Barone, V.; Mennucci, B.; Cossi, M.; Scalmani, G.; Rega, N.; Petersson, G.A.; Nakatsuji, H.; Hada, M.; Ehara, M.; Toyota, K.; Fukuda, R.; Hasegawa, J.; Ishida, M.; Nakajima, T.; Honda, Y.; Kitao, O.; Nakai, H.; Klene, M.; Li, X.; Knox, J:E.; Hratchian, H.P.; Cross, J.B.; Bakken, V.; Adamo, C.; Jaramillo, J.; Gomperts, R.; Stratmann, R.E.; Yazyev, O.; Austin, A.J.; Cammi, R.; Pomelli, C.; Ochterski, J.W.; Ayala, P.Y.; Morokuma, K.; Voth, G.A.; Salvador, P.; Dannenberg, J.J.; Zakrzewski, V.G.; Dapprich, S.; Daniels, A.D.; Strain, M.C.; Farkas, O.; Malick, D.K.; Rabuck, A.D.; Raghavachari, K.; Foresman, J.B.; Ortiz, J.V.; Cui, Q.; Baboul, A.G.; Clifford, S.; Cioslowski, J.; Stefanov, B.B.; Liu, G.; Liashenko, A.; Piskorz, P.; Komaromi, I.; Martin, R.L.; Fox, D.J.; Keith, T.; Al-Laham, M.A.; Peng, C.Y.; Nanayakkara, A.; Challacombe, M.; Gill, P.M.W.; Johnson, B.; Chen, W.; Wong, M.W.; Gonzalez, C.; Pople, J.A.; *Gaussian 03, Revision C.02*; Gaussian, Inc.: Wallingford CT, **2004**.

(32) Nakamoto, K.; *Infrared and Raman Spectra of Inorganic and Coordination Compounds (5th Ed.)*, Wiley, New York, USA, 1997.

(33) Petrusenko, S.P.; Kokozey, V.N.; Simonov, Yu, A.; *Zh. Neorg. Khim. (Russ. J. Inorg. Chem.)*, **1994**, 39(1), 81.

(34) Sudbrake, C.; Vahrenkamp, H.; *Z. Anorg. Allg. Chem.*, **2001**, 627(5), 857–862.

(35) Hollingsworth, N.; Kanna, M.; Kociok-Kohn, G.; Molloy, K.C.; Wongnawa, S.; *Dalton Trans*, **2008**, 631–641.

(36) Ye, B.; Li, X.; Williams, I.D.; Chen, X.; *Inorg. Chem.*, **2002**, 41, 6426-6431.

(37) Allen, F.H.; *Acta Cryst. Sect. B*, **2002**, 58(3-1), 380–388.

(38) Eloussifi, H.; Farjas, J.; Roura, P.; Camps, J.; Dammak, M.; Ricart, S.; Puig, T.; Obradors, X.; *J. Therm. Anal. Calorim.*, **2012**, 108(2), 589–596.

(39) Farjas, J.; Camps, J.; Roura, P.; Ricart, S.; Puig, T.; Obradors, X.; *Thermochim. Acta*, **2011**, 521(1–2), 84–89.

(40) Farjas, J.; Camps, J.; Roura, P.; Ricart, S.; Puig, T.; Obradors, X.; *Thermochim. Acta*, **2012**, 544, 77–83.

(41) Roura, P.; Farjas, J.; Camps, J.; Ricart, S.; Albiol, J.; Puig, T.; Obradors, X.; *J. Nanopart. Res.*, **2011**, 13, 4085–4096.

(42) Bouchoux, G.; Choret, N.; Berruyer-Penaud, F.; Flammang, R.; *Int. J. Mass Spectrometry*, **2002**, 217(1), 195–230.

(43) Roura, P.; Farjas, J.; Eloussifi, H.; Carreras, L.; Ricart, S.; Puig, T.; Obradors, X.; *Thermochim. Acta*, **2015**, 601, 1–8.

(44) NIST X-ray Photoelectron Spectroscopy Database, http://srdata.nist.gov/xps/.

(45) Kim, Y-S.; Tai, W-P.; Shu, S-J.; *Thin Solid Films*, **2005**, 491(1–2), 153–160.

(46) Yang, L.; Zhao, Q.; Willander, M.; Liu, X.; Fahlman, M.; Yang, J.H.; *Appl. Surf. Sci.*, **2010**, 11 (256), 3592-3597.